CHAPTER II
LITERATURE REVIEW

2.1 Bacterial Cellulose

The most abundant biopolymer on earth is cellulose. Not only its biosynthesis by plants, but also by animal, bacterial, chemical and enzymatic (Pecoraro *et al.*, 2007). Bacterial cellulose is synthesized by acetic acid bacterium Glucanacetobacter xylinus (also denominated as Acetobacter xylinum) (Yang *et al.*, 2012). It is identical to cellulose produced by plants, in regard to its molecular formula and polymeric structure, but bacterial cellulose presents a higher crystallinity, water absortion, and mechanical strength (Pecoraro *et al.*, 2007; Kurosumi *et al.*, 2009). Additionally, it differs from plant-derived cellulose by having no any impurity such as hemicellulose, pectin, and lignin (Kurosumi *et al.*, 2009). Table 2.1 compares some properties of plant cellulose and bacterial cellulose.

Table 2.1 Properties of plant (PC) and bacterial (BC) cellulose (Pecoraro *et al.*, 2007)

Properties	PC	BC
Fibre width	1.4-4.0x10^{-2} mm	70-80 nm
Crystallinity	56-65%	65-79%
Degree of Polymerization	13,000-14,000	2,000-6,000
Young's modulus	5.5-12.6 GPa	15-30 GPa
Water content	60%	98.5%

Bacterial cellulose structure is a distinctive 3-D structure which consists of an ultrafme network of cellulose nanofibers (Yang *et al.*, 2012). These nanofibers are ribbon-like structures and made up of bundles of cellulose microfibrils (Torres *et al.*, 2012). Figure 2.1 (a) and (b) shows the raw bacterial cellulose hydrogels and the freeze-dried bacterial cellulose aerogels respectively. Figure 2.1 (c) demonstrates the FE-SEM image of a bacterial cellulose network. Figure 2.1 (d) illustrates a scheme of

the hierarchical structure of a bacterial cellulose fiber, from the basic glucose chain to the crystalline micro fibril and cellulose fiber (Yang, 2012). Therefore, it possesses unique properties due to this micromorphology. Figure 2.2 also shows three-dimensional network structure with entangled fibers of bacterial cellulose (Hu *et al.*, 2010).

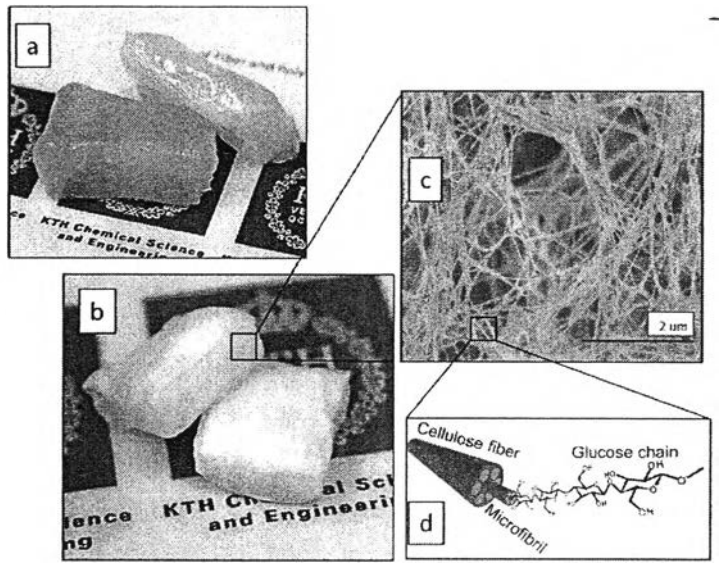

Figure 2.1 (a) Raw bacterial cellulose hydrogels, (b) freeze-dried bacterial cellulose aerogel, (c) FE-SEM picture of cross section from bacterial cellulose aerogel, (d) scheme of bacterial cellulose fibrils structure: glucose chains, micro fibrils, and cellulose fibers (Yang, 2012).

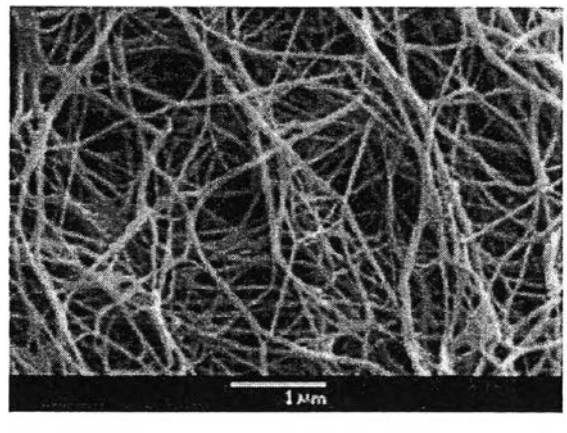

Figure 2.2 The SEM image of bacterial cellulose (Hu *et al.*, 2010).

Moreover, the intra and intermolecular hydrogen bonds of bacterial cellulose provide the parallel orientation and rigidity of bacterial cellulose structure as well as hydrophilic property which is shown in figure 2.3 (Pecoraro *et al.*, 2007).

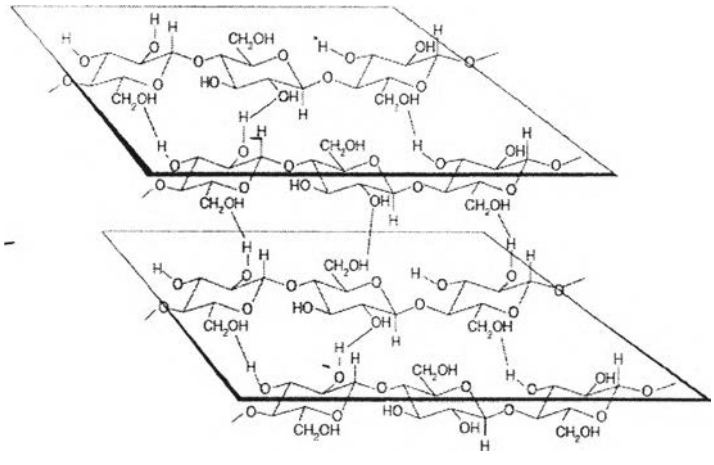

Figure 2.3 Intra- and inter-molecular hydrogen bonds among cellulose chains (Pecoraro *et al.*, 2007).

Pecoraro *et al.* (2007) shows FTIR spectrum of bacterial cellulose membrane (figure 2.4). The functional groups of bacterial cellulose are shown in table 2.2.

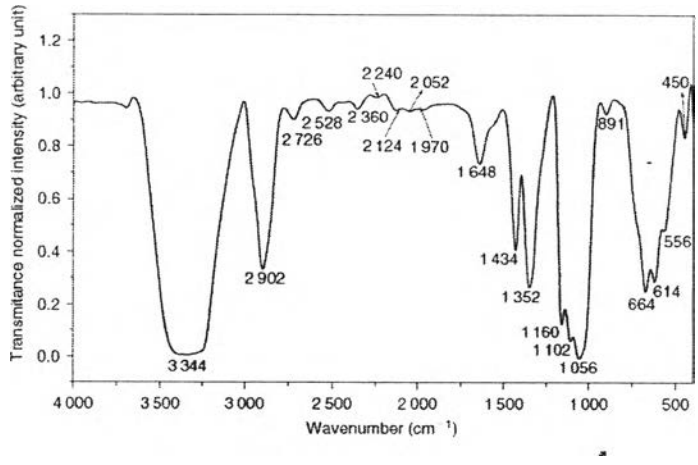

Figure 2.4 FTIR spectrum of a 200-μm thick bacterial cellulose membrane (Pecoraro *et al.*, 2007).

Table 2.2 Typical infrared absorption frequencies for bacterial cellulose (Pecoraro *et al.*, 2007)

Range (cm^{-1})	Assignment[a]
3 500–3 300	ν OH
3 000–2 870	ν CH and CH_2 (CHOH; CH_2OH)
1 645	δ_s HOH
1 430–1 330	δ C—OH e CH
1 200–1 000	ν C—O (—C—O—H)
1 150–1 000	ν C—O (C—O—C)
900–700	δ_{as} in plane CH_2
	δ C—H
700–400	δ out of the plane OH

[a] ν = stretching; δ = angular bending; s = symmetric; as = asymmetric.

They also shows the X-ray diffractogram of bacterial cellulose (figure 2.5) which indicates the presence of crystalline peaks and amorphous regions. They claim that it is impossible to separate the contribution of each one on the peak at approximately 2Θ = 15° and 23°. The peak at 15° corresponds to the diffractions from triclinic (100) and monoclinic (110) planes, whereas the peak at 23° corresponds to the reflections from triclinic (110) and monoclinic (200) planes.

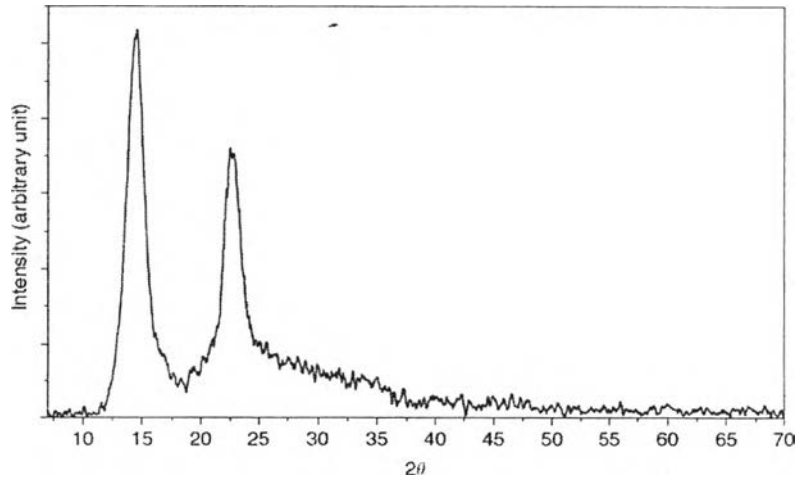

Figure 2.5 X -ray diffractogram of a bacterial cellulose membrane. The sample was supported on a borosilicate glass holder (Pecoraro *et al.*, 2007).

2.2 Applications of Bacterial Cellulose

Bacterial cellulose synthesized by Acetobacter xylinum is an outstanding biomaterial which possesses unique properties, including high crystallinity, ultrafine fiber network, high tensile strength in the wet state and the capability to be formed into three-dimensional structure during synthesis. Additionally, porous bacterial cellulose could be derived from freeze-drying process. It composes of nanofibrils with hierarchical pore structure consisting of large pores (20~1000 μm in diameter) and nanopores (down to ~4 nm diameter). It has high surface area (92.81±2.02 m^2/g) and adequate porosity (90.42 ±0.24%) (Gao *et al.*, 2011).

Because of its prominent mechanical properties, conformability and porosity, consequently, bacterial cellulose has been widely used in a number of applications (Torres *et al.*, 2012). Table 2.3 summarized some applications of bacterial cellulose.

Table 2.3 Examples of applications of bacterial cellulose (Pecoraro *et al.*, 2007)

Area	Application
Cosmetics	Stabilizer of emulsions; component of artificial nails
Textile industry	Artificial textiles; highly absorbent materials
Sports and tourism	Sporting clothes; tents; camping material
Mining and refinery	Sponges for recovery spilled oil; material for toxin adsorption
Wastes treatment	Recycling of minerals and oils
Sewage purification	Urban sewage purification; water ultrafiltration
Broadcasting	Sensitive diaphragms for microphones and stereo headphones

Forestry	Artificial wood replacer, multi-layer plywood, heavy-duty containers
Paper industry	Specialty papers, archival documents repairing, more durable banknotes, diapers, napkins
Machine industry	Car bodies, airplane parts, sealing of cracks in rocket casings
Food production	Edible cellulose (Nata de coco)
Medicine	Temporary artificial skin for therapy of burns and ulcers, component of dental implants
Laboratory	Immobilization of proteins, cells; chromatographic techniques; medium for tissue cultures
New applications	Cellulose thin films for documents and book recovery; fibres (including optical); biodegradable plastics; oriented templates; liquid crystal displays; luminescent materials; fuel cell membranes; drug delivery; stents covering; ophthalmic, cardiovascular and neurological prostheses; bulletproof materials

Dubey *et al.* (2002) prepared bacterial cellulose as a membrane for dehydration of ethanol. The medium for cellulose production from Acetobacter xylinum is shown in table 2.4. These membranes have high amount of proteins and cellulose. Some of these membranes were soaked for 48 hours in saturated solution of NaOH. NaOH solubilizes the proteinaceous matter from the membrane, only a cellulosic matrix remains in the membrane. NaOH treated membrane is also called

deproteinated membrane. After that these membranes were rinsed with distilled water until the pH of drained liquid was neutral and then dried at ambient conditions.

Table 2.4 Medium for cellulose production from Acetobacter xylinum (Dubey *et al.*, 2002)

Chemical	Concentration (g/l)
Sucrose	50.0
Yeast extract	5.0
Ammonium sulphate	5.0
Potassium hydrogen phosphate	3.0
Magnesium sulphate, hydrated	0.05

They found that the amide bond at 1538 cm^{-1} disappeared when bacterial cellulose was treated with sodium hydroxide solution (figure 2.6). That means only a cellulosic matrix remains in the membrane.

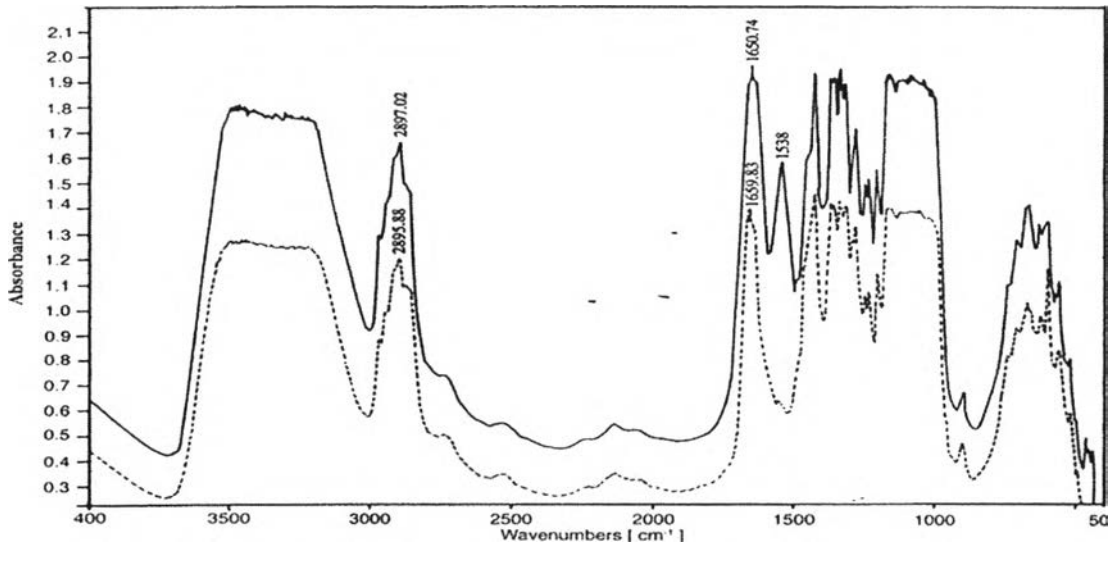

Figure 2.6 FTIR spectra of nascent and NaOH treated BCM (Dubey *et al.*, 2002).

From tensile testing results, they claimed that bacterial cellulose membrane has high tensile properties as can be seen in table 2.5. Moreover, these bacterial cellulose membrane also has high chemical resistance. It is insoluble in alcohols, ketones, aldehydes, hydrocarbons, ether, aprotic solvents (DMF, DMSO, THF) as well as dilute acids and bases. However, it swells in water without dissolution.

Table 2.5 Mechanical properties of NaOH treated BCM (Dubey *et al.*, 2002)

Property	Mean value	Standard deviation (S.D.)
Strain @ break (%)	10.50	1.58
Elongation @ break (mm)	3.33	0.54
Stress @ break (Nmm^{-2})	0.1	0.03
Young's Modulus (Nmm^{-2})	101.6	0.96

Furthermore, they observed that the sorption selectivity values were favored when the feed was richer in ethanol and contained 30–50% of water by volume. The membrane was found highly selective to water. Even when the feed was rich in ethanol (>70% (w/w)) the permeate contained higher than 95% (w/w) of water. It indicates that the bacterial cellulose membrane is hydrophilic in nature and adsorbs almost seven times more water than alcohol.

Pandey *et al.* (2005) also fabricated bacterial cellulose membranes for pervaporative separation of aqueous organic mixtures. The chosen organics for their study are acetone (AC), formalin (HCHO), ethanol (EtOH), ethylene glycol (EG) and glycerol (Gly). They found that the highest of flux were obtained from $EtOH/H_2O$ system which increased with the increasing of organic concentration in the feed mixtures. This hydrophilic bacterial cellulose membrane presents a high sorption ability for organics e.g. Gly and EG. These organics can form extensive hydrogen bonding with the cellulose molecules in the membrane. Highest selectivity was obtained from a mixture of glycerol with 40% (v/v) water, in contrast, a mixture of ethanol with 40% (v/v) water showed the lowest selectivity. Generally, the plasticization of the membrane occurs when there are water molecules in the aqueous

binary mixtures of organic chemicals, which increases overall sorption. This membrane prefers to sorb water from the binary mixtures.

2.3 Natural Gas

Natural gas is an alternative energy which is a vital component of the world's supply of energy. It has widely variable compositions as shown in table 2.6, however, its compositions depend on the geological area and the underground deposit type, depth and location (Yeo *et al.*, 2012). For this reason, after natural gas comes out of the ground, it goes to a processing plant in order to clean of impurity and separate into various components. Gas dehydration and gas sweetening are two crucial processes in raw natural gas processing. The research attention in gas sweetening has been attended to the removal of CO_2 owing to its high amount in the raw natural gas than H_2S. The removal of CO_2 will enhance the energy content (calorific value) of natural gas, decrease volume in the pipeline and pipeline corrosion. Although, cryogenic distillation, adsorption and membrane separation are generally used for CO_2 removal, membrane separation technique has several advantages over other techniques. The growth rate of membrane separation is higher than any of these aforementioned methods (Adewole *et al.*, 2013). Therefore, membrane separation technology was used for CO_2 separation in this study.

Table 2.6 Typical natural gas compositions (Adewole *et al.*, 2013)

Component	Composition range (mol%)
Helium	0.0-1.8
Nitrogen	0.21-26.10
Carbon dioxide	0.06-42.66
Hydrogen sulfide	0.0-3.3
Methane	29.98-90.12
Ethane	0.55-14.22
Propane	0.23-12.54

Butanes	0.14-8.12
Pentanes and heavier	0.037-3.0

2.4 Membrane for Gas Separation

Membranes in the separation process act as barriers for separating one or more gases from a feed mixture. The membrane_performance is evaluated by two characteristics which are gas permeance and selectivity. Gas permeance is the amount of gas (in moles) which goes through a membrane of known area per unit time per cross-membrane pressure as shown in the following equation:

$$\left(\frac{P}{\delta}\right)_i = \frac{Q_i \, x \, 14.7x10^6}{(A)x(\Delta P)x76}$$

Selectivity is defined as the ratio of permeance of each component which can be expressed by the following equation:

$S_{A/B} = P_A / P_B$

Gas separation processes require a membrane with high permeability and selectivity.

The membrane gas separation process offer a number of advantages (Iarikov *et al.*, 2011).

i) Low capital investment

ii) High energy efficiency

iii) High process flexibility

iv) Low space requirement

v) Environmental friendly

Membrane structures can be classified according to the cross-section microstructure, which can be divided into 2 types; symmetrical and asymmetrical membrane (figure 2.7). Symmetrical membranes have a nearly homogeneous structure all over the thickness of the membrane, while asymmetrical membranes consist of two layers: the top one is a very thin dense layer and the bottom one is a porous sub-layer (Abedini *et al.*, 2010). Bacterial cellulose membrane is a symmetrical membrane.

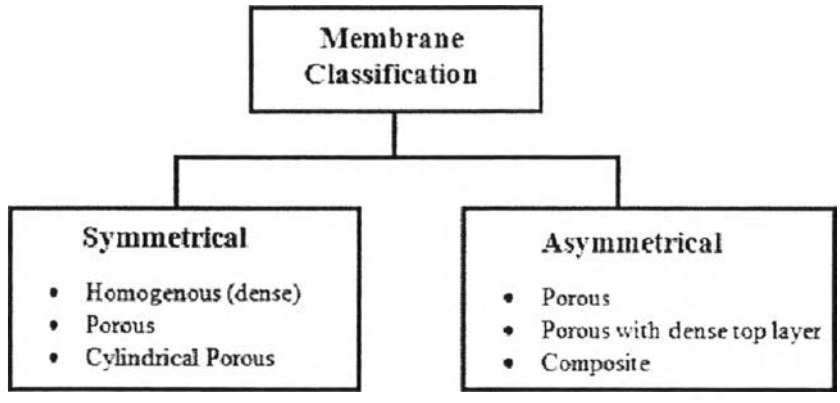

Figure 2.7 Membrane classifications (Abedini *et al.*, 2010).

Ito *et al.* (1997) studied the gas permeation through a water-swollen chitosan membrane. A feed saturated water vapor will make hydrophilic membrane into a swollen state. They found that the permeation rate of a dry chitosan membrane was too low to measure. It reached a steady state after 50 hours. They found that large gas permeability was obtained when a water-swollen chitosan membrane was used. Carbon dioxide preferentially permeated through the swollen chitosan membrane with a permeability of $2.5\times10^{-8}cm^3(STP)\cdot cm/(s\cdot cm^2\cdot cmHg)$ and a CO_2/N_2 separation factor of 70 at room temperature. This separation performance for CO_2 resulted from a basic property of the amino groups in the chitosan molecules.

Xing *et al.* (2009) investigated the gas separation performance using crosslinked polyvinylalcohol (PVA)/polyethyleneglycol (PEG) blend membranes. They could achieve high CO_2/CH_4 selectivity for this membrane as a result of the polar segments in the membrane. In addition, PVA provides a mechanically strong polymer matrix. They conducted the gas permeation experiments by using the feed gas with composition of 50%CO_2 and 50%CH_4. The gas flow rates of the feed were 60 cc/minutes.

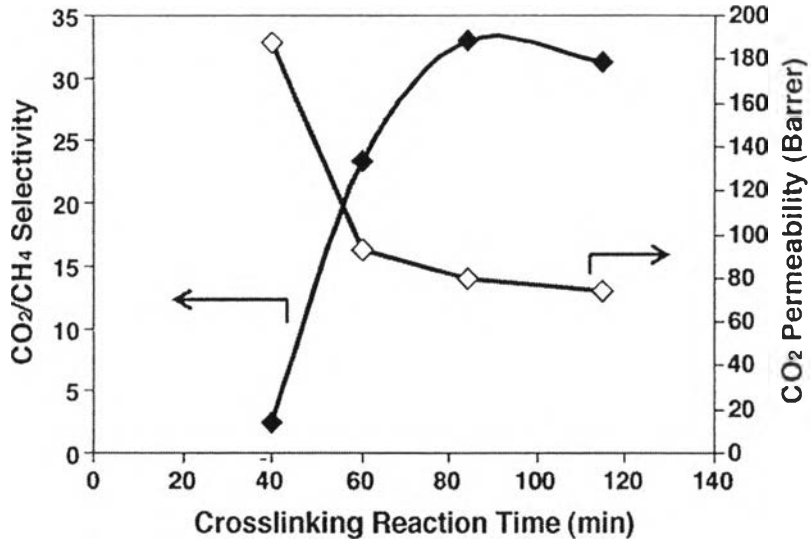

Figure 2.8 Effect of the crosslinking time on CO_2/CH_4 separation performance for the polymer blend of 36 wt.% PVA and 64 wt.% PEG (MW 200) at 30°C.

Figure 2.8 shows that the crosslinking time has an effect to the separation performance. When the crosslinking time increased from 84 to 120 minutes, the CO_2/CH_4 selectivity decreased because of the loss of hydroxyl groups. Furthermore, they found that the increase of the crosslinking time from 40 to 120 minutes resulted in a continuous decrease in CO_2 permeability due to the reduced chain mobility and the increased densification of the polymer chains.

Basu *et al.* (2010) prepared Matrimid®, polysulphone (PSf) and their blends with different ratios (Matrimid®/PSf : 1/3, 1/1 and 3/1) for using as the gas separation asymmetric membranes. Binary gas mixture selectivities and permeances for CH_4 and CO_2 were investigated. The effective membrane area is 2.24 cm^2. They studied the effect of CO_2 feed composition, temperature, pressure and time on a binary gas mixture performance. They found that the blend membranes show better stability at high CO_2 feed composition, higher pressure and elevated temperature than the Matrimid® membrane.

2.5 Mechanisms for Gas Separation

Mechanisms for gas separation depend on the properties of the permeate and the membrane (Pandey *et al.*, 2001). There are five possible mechanisms; Knudson diffusion, molecular sieving, solution-diffusion separation, surface diffusion and capillary condensation, of which the first three are schematically represented in figure 2.9, 2.10 and 2.11. In Knudsen diffusion, gas components are separated based on the difference in the mean path of the gas molecules due to collisions with the pore walls, which is related to the molecular weight (table 2.5). In molecular sieving, gas components are separated based on size exclusion, the size being the kinetic diameter of the gas molecules. Solution-diffusion, the gases are separated by their solubility within the membrane and their diffusions through the membrane matrix (Scholes *et al.*, 2008).

Table 2.7 Molecular Weight (Da) and Kinetic Diameter (A°) of Gase (Scholes *et al.*, 2008)

Molecule	Molecular Weight	Kinetic Diameter(A°)
CO_2	44	3.3
O_2	32	3.46
N_2	28	3.64
H_2O	18	2.65
CH_4	16	3.8
H_2	2	2.89

2.5.1 Knudsen Diffusion

Knudsen diffusion separation is based on gas molecules passing through membrane pores that is small enough to prevent bulk diffusion (Scholes *et al.*, 2008). Especially, at low pressure, collisions are notably between gas molecules and the walls. In this regime, termed Knudsen diffusion, the presence of other gases no longer affects the transport, and the flux depends only on the density gradient of

the species of interest and can be written as (Mason and Malinauskas, 1983):

$$J_i = -D_K \frac{\partial \rho_1}{\partial z}$$

Besides the flux, the selectivity for any gas pair is determined by the inverse ratio of the square root of their molecular weight (Scholes *et al.*, 2008).

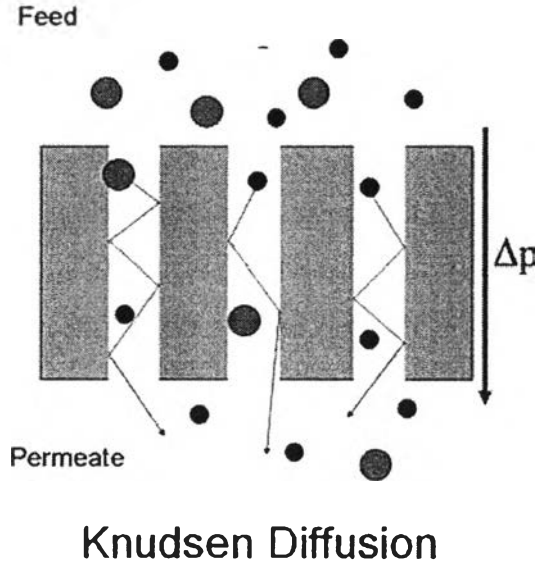

Figure 2.9 Schematic representation of Knudsen diffusion (Scholes *et al.*, 2008).

2.5.2 Molecular Sieving

Molecular sieving is found on the size exclusion for separating gas mixtures. Pores within the membrane are controlled the size relative to the kinetic diameter of the gas molecule. This allows diffusion of smaller gases at a much faster rate than larger gas molecules (Scholes *et al.*, 2008).

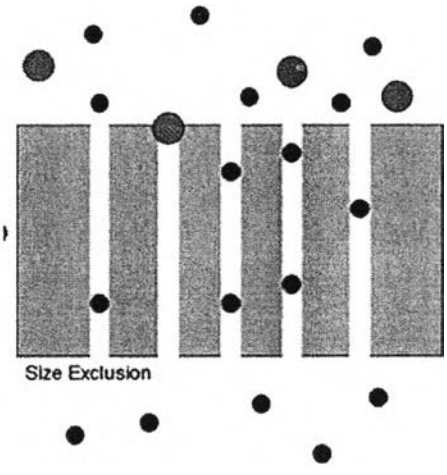

Figure 2.10 Schematic representation of molecular sieving (Scholes *et al.*, 2008).

2.5.3 Solution-Diffusion Mechanism

The principal of the solution-diffusion model is about the dissolution of the permeate in the membrane material and then diffuse through the membrane down a concentration gradient (Wijmans *et al.*, 1995).

The solution-diffusion mechanism composes of three steps.

i) absorption or adsorption at the feed surface

ii) solubility through the membrane

iii) desorption on the permeating side

The differences in the amount of permeate diffusing through the membrane cause the differences in the permeance which acquire a separation. The rate determining parameter of gas transport through the membrane is the permeability coefficient which can be expressed by the following equation:

$$P = DS,$$

where P is the permeability coefficient, D the diffusion coefficient, and S the solubility coefficient (Pandey *et al.*, 2001). The selectivity of a membrane to separate gas component *i* and *j* is defined by their permeability ratio as:

$$\alpha_{\frac{i}{j}} = \frac{P_i}{P_j} = \left(\frac{D_i}{D_j}\right)\left(\frac{S_i}{S_j}\right),$$

where D_i/D_j is the diffusion selectivity and S_i/S_j is the solubility selectivity.

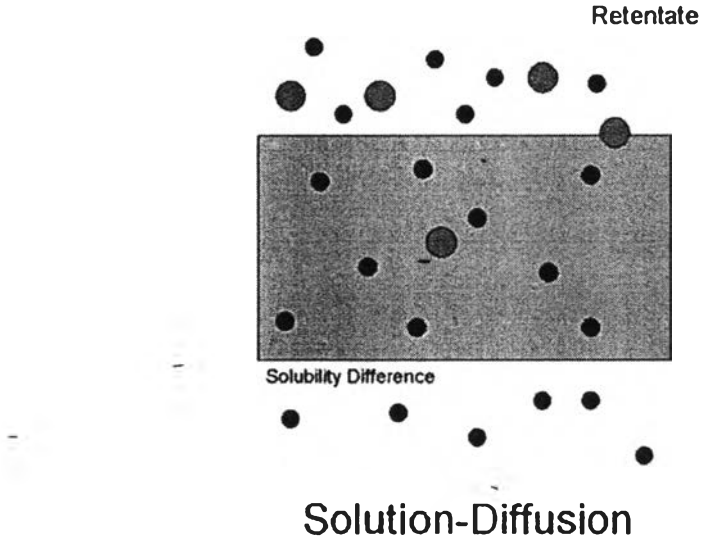

Figure 2.11 Schematic representation of solution-diffusion (Scholes *et al.*, 2008).

2.6 Facilitated Transport Membrane

Facilitated transport membranes have been attractive because of their potential to achieve high both permeability and selectivity, whereas many polymeric membranes generally only improve the permeability or selectivity (Mun *et al.*, 2009). These membranes incorporated with transition metal ions that used as carriers for olefin transport due to their capacity to react specifically and reversibly with unsaturated molecules (Pollo *et al.*, 2012). Figure 2.12 shows the model of π-complexation for the interaction between double bond of the olefin and the transition metal ions.

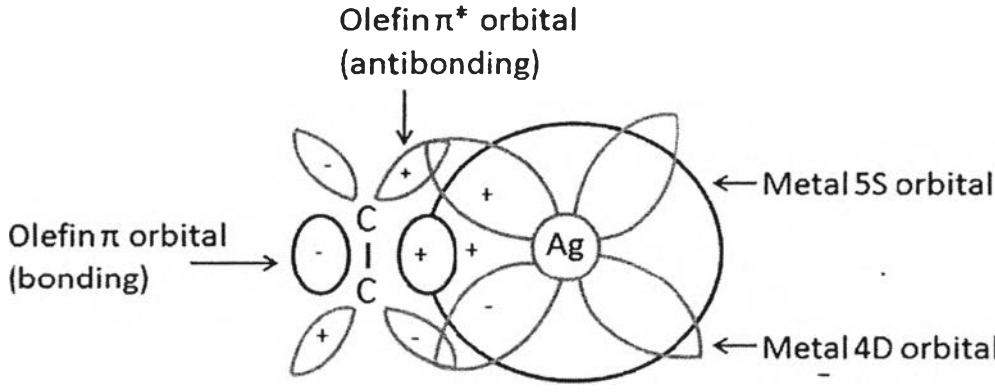

Figure 2.12 π-complexation between olefins and silver metal ions (Faiz *et al.*, 2012).

This complexation reaction begins with the formation of a sigma-type donation bond from the filled π-orbitals of the olefin to the empty s-orbital of the metal, followed by a π back-donation bond from the filled d-orbitals of the metal to the empty π*-orbital of the olefin. The stability of this complex depends on electronic and steric factors. The bond strength between the metal ions and the olefin must be weak enough for the ability of transportation of the olefin towards the permeate side (Cotton *et al.*, 1995). Silver and copper ions are mainly used as carrier agents for olefin separation because the π-complexation between olefins and silver/copper metal ions has lower stability in comparison with the π-complexes formed with other transition metals (Pollo *et al.*, 2012).

Facilitated transport membranes can be separated into two types which are mobile-carrier membranes and fixed-carrier membranes. The carrier can diffuse in the membrane in case of mobile-carrier membranes. On the other hand, the reactive carrier agents are covalently bonded to the polymer chain in case of fixed-carrier membranes. Therefore, CO_2 could react at one carrier site and then hops to the next site along the direction of the concentration driving force by hopping mechanism. Fixed-carrier membranes are more stable than mobile-carrier membranes since mobile-carrier membranes can be dried out and the carrier agents can be lost (Huang *et al.*, 2008).

Nicharat *et al.* (M.S.Thesis) studied the effect of adding silver ions into a novel organic polybenzoxazine xerogel (PBZ) as a membrane for flue gas separation. They found that the permeance values are higher when the molecular kinetic diameters of gas molecules are higher (figure 2.13) as the larger molecules are hardly enter the pores, hence, these molecules can come out first. On the other hand, the smaller molecules have more complex pathways to exit as shown in figure 2.14.

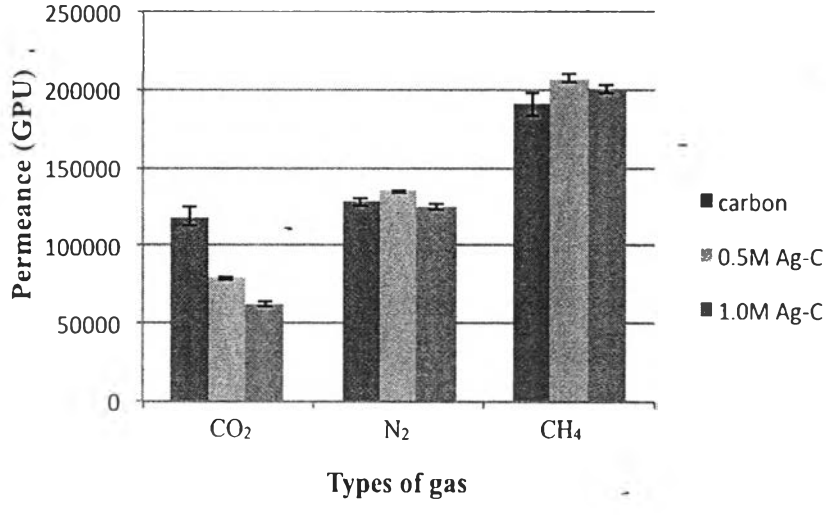

Figure 2.13 Effects of Silver Nitrate concentration on CO_2, CH_4 and N_2 permeability.

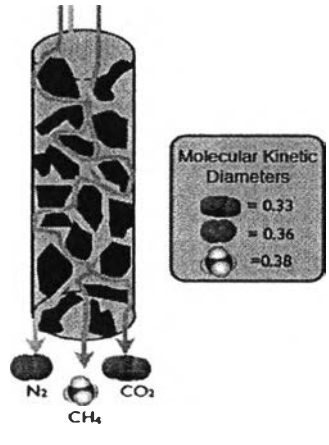

Figure 2.14 Pathway of gases depending on molecular kinetic diameter.

Furthermore, they also found that the CO_2 /CH_4 selectivity increased obviously when silver ions present in the membranes (figure 2.15) because CO_2 molecules have double bonds could react reversibly with these silver ions to form the π-complexation results in good separation performance.

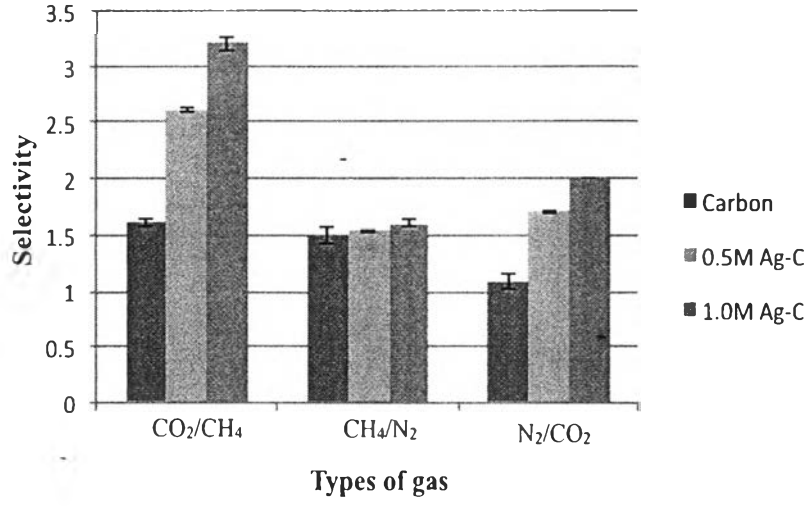

Figure 2.15 Effects of silver inclusion on CO_2/CH_4, CH_4/N_2 and N_2/CO_2 selectivity.

Ryu *et al.* 2001 examined the separation performance of ethylene/ethane and propylene/propane mixtures through a dry complex membrane $AgBF_4$-cellulose acetate. They achieved the maximum selectivity for olefin over paraffin was 280 for the ethylene/ethane mixture and 200 for the propylene/propane mixture. In their work, silver ions were coordinated with carbonyl oxygen atoms among three different types of oxygen atoms present in cellulose acetate which was clearly illustrate by FTIR and XPS studies. Hence, they found the carbonyl stretching frequency of the free cellulose acetate at 1750 cm^{-1} shifts to a lower frequency by about 41 $cm^{-1}$when cellulose acetate incorporated with $AgBF_4$. In addition, the binding energy corresponding to a carbonyl oxygen atom in the O 1s XPS spectrum shifts to a more positive binding energy by the incorporation of $AgBF_4$.

Pollo *et al.* (2012) investigated the effects of adding silver salts to PU membranes and evaluated their performance for the separation of propylene/propane mixtures. The gas separation experiments were undertaken at a feed pressure and

temperature of 2 bar and 25°C, respectively. The results of these experiments are summarized in table 2.8. It can be observed that the presence of the silver salt in PU membranes promotes an increase in the ideal selectivity.

Table 2.8 Gas permeance and separation factor of propylene and propane through PU membranes

Membrane	Gas Permeance (Barrer)		$\alpha_{C3H6/C3H8}$
	Propylene	Propane	
Pure PU	191.5	91.6	2.1
PU/$AgCF_3SO_3$ (20% w/w)	188.1	18.0	10.4
PU/$AgSbF_6$ (20 % w/w)	50.1	7.7	6.5

From FTIR spectra (figure 2.16), they discovered the band position of hydrogen bonded -NH slight shift from 3328 cm^{-1} for PU to 3323 cm^{-1} for PU/$AgCF_3SO_3$. It shifts to lower wavenumbers because of the coordination of silver ion with the hydrogen bonded –NH group. Figure 2.17 also shows a slight shift of ester oxygen region from 1166 cm^{-1} for PU to 1160 cm^{-1} for PU/ $AgCF_3SO_3$.

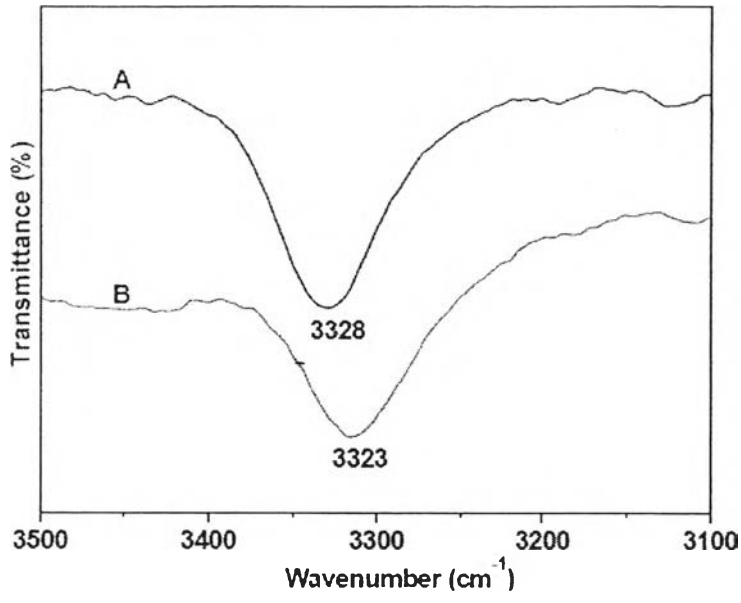

Figure 2.16 FTIR spectra of PU film (A) and PU/$AgCF_3SO_3$ (20% w/w) (B) in the hydrogen bonded NH region.

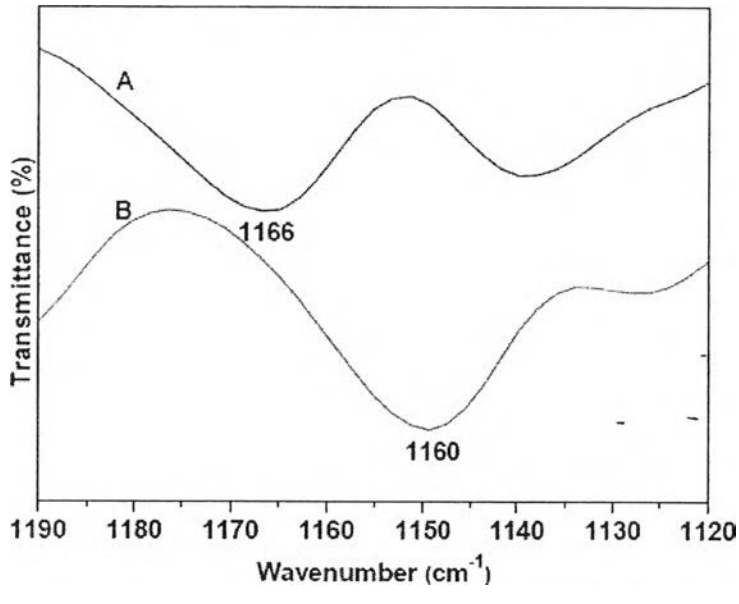

Figure 2.17 FTIR spectra of PU film (A) and PU/$AgCF_3SO_3$ (20% w/w) (B) in the ester region.